Zigzag antiferromagnetic ground state with anisotropic correlation lengths in the quasi-two-dimensional honeycomb lattice compound Na$_2$Co$_2$TeO$_6$

A. K. Bera, S. M. Yusuf,[*] and Amit Kumar

Solid State Physics Division, Bhabha Atomic Research Centre, Mumbai 400085, India

C. Ritter

Institut Laue-Langevin, 71 Avenue des Martyrs, 38000 Grenoble, France

The crystal structure, magnetic ground state, and the temperature-dependent microscopic spin-spin correlations of the frustrated honeycomb lattice antiferromagnet Na$_2$Co$_2$TeO$_6$ have been investigated by powder neutron diffraction. A long-range antiferromagnetic (AFM) ordering has been found below $T_N \sim 24.8$ K. The magnetic ground state, determined to be zigzag antiferromagnetic and characterized by a propagation vector $\mathbf{k} = (1/2\,0\,0)$, occurs due to the competing exchange interactions up to third-nearest neighbors within the honeycomb lattice. The exceptional existence of a limited magnetic correlation length along the c axis (perpendicular to the honeycomb layers in the ab planes) has been found even at 1.8 K, well below the $T_N \sim 24.8$ K. The observed limited correlation along the c axis is explained by the disorder distribution of the Na ions within the intermediate layers between honeycomb planes. The reduced ordered moments $m_{Co(1)} = 2.77(3)\,\mu_B/Co^{2+}$ and $m_{Co(2)} = 2.45(2)\,\mu_B/Co^{2+}$ at 1.8 K reflect the persistence of spin fluctuations in the ordered state. Above $T_N \sim 24.8$ K, the presence of short-range magnetic correlations, manifested by broad diffuse magnetic peaks in the diffraction patterns, has been found. Reverse Monte Carlo analysis of the experimental diffuse magnetic scattering data reveals that the spin correlations are mainly confined within the two-dimensional honeycomb layers (ab plane) with a correlation length of ~ 12 Å at 25 K. The nature of the spin arrangements is found to be similar in both the short-range and long-range ordered magnetic states. This implies that the short-range correlation grows with decreasing temperature and leads to the zigzag AFM ordering at $T \leqslant T_N$. The present study provides a comprehensive picture of the magnetic correlations over the temperature range above and below the T_N and their relation to the crystal structure. The role of intermediate soft Na layers on the magnetic coupling between honeycomb planes is discussed.

I. INTRODUCTION

The investigation of novel quantum states, tailored by strong quantum fluctuations and/or strong frustration, in low-dimensional spin systems has been an active research field in recent years. In this respect, the two-dimensional (2D) honeycomb lattice model is of special interest, as it has the lowest coordination number ($z = 3$) in two dimensions, hence, the strongest possible quantum fluctuations. Unlike 2D triangular and kagome lattices, the honeycomb lattice with only nearest-neighbor (NN) exchange interaction (J_1) does not show geometrical spin frustration and has a Néel antiferromagnetic (AFM) ground state in the classical limit ($S \rightarrow \infty$). However, frustration can be easily introduced in a honeycomb lattice by inclusion of competing next-nearest-neighbor (NNN) (J_2) and/or next-next-nearest-neighbor (NNNN) (J_3) exchange interactions. This frustrated model with J_1, J_2, and J_3 has been known to possess a massive degeneracy of the magnetic ground state, which, however, might be lifted either due to quantum or thermal fluctuations, the effect known as "order by disorder," leading to exotic ordered magnetic states and a complex magnetic phase diagram. Depending on the signs and ratios of the exchange interactions (J_2/J_1 and J_3/J_1) and the spin values, different types of ordered and quantum disordered magnetic phases are theoretically proposed for the honeycomb

lattices. These include Néel, zigzag, stripy, and spiral/helical ordered states, as well as disordered quantum spin liquid and quantum paramagnetic (plaquette valence bond state) states [1–8]. Moreover, the presence of an interplanar exchange coupling between honeycomb layers can qualitatively change the microscopic nature of the magnetic ground states [9]. Furthermore, the honeycomb lattice spin systems show diverse phenomena, such as topological phase transitions (also known as Kosterlitz-Thouless transition) [10], superconductivity [11], and gapless quantum spin liquid [12]. A possible realization of the highly frustrated Kitaev-Heisenberg model has also been proposed for the honeycomb lattice [13].

Experimental efforts have been undertaken to explore and understand the unique properties of frustrated honeycomb lattice compounds. The family of compounds BaM_2(XO$_4$)$_2$ with M = Co and Ni, and X = P and As forms weakly coupled frustrated honeycomb lattices of magnetic ions M with spin $S = 1/2$ for Co, and $S = 1$ for Ni. In BaCo$_2$(AsO$_4$)$_2$, the cobalt moments order abruptly at $T_c = 5.4$ K with a helical magnetic structure [14], whereas the isostructural compounds BaNi$_2$(PO$_4$)$_2$ and BaNi$_2$(AsO$_4$)$_2$ show collinear AFM structures (stripy and zigzag AFM structures, respectively) below 24.05 and 18.65 K, respectively, [15]. The honeycomb lattice delafossite compounds Cu$_3$Ni$_2$SbO$_6$ and Cu$_3$Co$_2$SbO$_6$ show zigzag AFM ordering in the honeycomb plane [16]. On the other hand, in the $S = 3/2$ honeycomb Heisenberg compound Bi$_3$Mn$_4$O$_{12}$(NO$_3$) no long-range magnetic order is present due to the competing interactions between the J_1

*smyusuf@barc.gov.in

and J_2 [12,17,18]. Moreover, a commensurate Néel AFM long-range order state can be induced in $Bi_3Mn_4O_{12}(NO_3)$ by an application of a magnetic field [12,19]. Another honeycomb compound with $S = 1/2$, $InCu_{2/3}V_{1/3}O_3$, shows only short-range antiferromagnetic order within the 2D plane without any magnetic correlation between such planes along the c axis [20].

The newly discovered families of layered honeycomb lattice compounds with general formula $A_2^+ M_2^{2+} Te^{6+}O_6$ (P2-type crystal structure) and $A_3^+ M_2^{2+} X^{5+}O_6$ (O3-type crystal structure) (where $A = $ Ag, Li, and Na; $X = $ Bi and Sb; and M is a transition metal) [16,21–33] offer the possibility to study the role of signs and ratios of exchange interactions (J_2/J_1 and J_3/J_1), as well as of the spin value on the magnetic ground state and the magnetic properties. In these compounds, the honeycomb layers are formed by edge-sharing MO_6 octahedra with TeO_6 or XO_6 at the center of the honeycomb lattice. For magnetic ions M the network created by the edge-sharing MO_6 octahedra provides higher-order exchange interactions beyond the nearest neighbors within the honeycomb layers. The magnetic honeycomb layers are separated by the nonmagnetic layers of Na/Li/Ag. In these crystal structures, the Na and Li atoms are very diffusive leading to the compounds being suitable as cathode materials in heavy ion rechargeable batteries. At the same time, the crystal structures are soft due to the intermediate Na/Li layers, and provide an easier and effective control of the interlayer magnetic couplings, hence, a tuning of magnetic lattice dimensionality. Among the experimentally studied compounds from the above series, a spin-gap behavior was found for the Cu^{2+} $(S = 1/2)$ based compounds $Na_2Cu_2TeO_6$ [22] and $Na_3Cu_2SbO_6$ [23]. Absence of long-range magnetic ordering was reported for the structurally similar compounds $Na_3LiFeSbO_6$, Na_4FeSbO_6, and Li_4MnSbO_6 [34,35], and was related to disorder and frustration effects. Recently, density functional theory (DFT) calculations proposed a long-range zigzag AFM ordering for the compounds $(Li/Na)_3Ni_2SbO_6$ [30]. Recently, a long-range zigzag AFM ordering was reported experimentally on $Na_3Co_2SbO_6$ [31]. An AFM ordering at low temperatures was also reported for the O3-type honeycomb compounds $Na_3M_2SbO_6$ ($M = $ Cu and Ni) [16,36,37], $A_3Ni_2BiO_6$ with $A = $ Na and Li [25,38], and $Li_3Ni_2SbO_6$ [24], as well as for the P2-type compounds $Na_2M_2TeO_6$ ($M = $ Co and Ni) [36,37,39]; however, their real quantum ground states remain unknown and await for an experimental investigation. The influence of the intermediate soft Na/Li layers on the magnetic correlations also remains unexplored in these systems.

In view of this, the bilayer honeycomb lattice compound $Na_2Co_2TeO_6$ is of present interest. Only the crystal structure and very basic bulk magnetic properties were reported for this compound in the literature [37,39], which reveal that $Na_2Co_2TeO_6$ orders antiferromagnetically at low temperatures without giving any details of the microscopic nature of the magnetic ground state. Here, we report the microscopic nature of the magnetic ground state, and a detailed temperature evolution of the magnetic correlations of $Na_2Co_2TeO_6$, both studied by neutron powder diffraction. The magnetic ground state is determined to be a zigzag antiferromagnet having—even deep into the long-range ordered state (down to 1.8 K)—a restricted correlation length perpendicular to the honeycomb layers.

The broken magnetic connections between the honeycomb layers are explained on the basis of the Na disorder in the interconnecting soft Na layers. The analysis by the reverse Monte Carlo (RMC) method of the diffuse magnetic scattering, observed above T_N, reveals a 2D short-range ordering with ferromagnetic (FM) NN, AFM NNN, and AFM NNNN correlations within the honeycomb planes. The present study provides a thorough characterization of magnetic correlations above and below the T_N, and their correlation to the crystal structure.

II. EXPERIMENTAL DETAILS

Polycrystalline samples of $Na_2Co_2TeO_6$ were synthesized by solid-state reaction. A stoichiometric mixture of Na_2CO_3 (99.9%), Co_3O_4 (99.99%), and TeO_2 (99.99%) was heated at $850\,^\circ$C in air for a total period of 94 h with several intermediate grindings.

The powder x-ray diffraction pattern was recorded using CuK_α radiation at room temperature. The ac susceptibility measurements were carried out using a commercial magnetometer (Cryogenic Co. Ltd., UK) under an ac field amplitude of 5 Oe, and a frequency of 987 Hz. Temperature-dependent heat capacity was measured by an ac calorimeter (Cryogenic). The dc magnetization measurements were carried out using a commercial vibrating sample magnetometer (Cryogenic Co. Ltd., UK). The temperature-dependent magnetization curves $[M(T)]$ were recorded under a 200 Oe magnetic field in the warming cycles over the temperature range of 1.5–300 K in zero-field-cooled (ZFC) and field-cooled (FC) conditions. Isothermal magnetizations were measured by a vibrating sample magnetometer (Cryogenic). A room-temperature neutron diffraction pattern was measured using the neutron powder diffractometer-II ($\lambda = 1.2443$ Å) at the Dhruva reactor, Bhabha Atomic Research Centre, Mumbai, India. Low-temperature neutron diffraction measurements were performed using the D1B ($\lambda = 2.524$ Å) and D20 ($\lambda = 2.41$ Å) powder diffractometers at the Institut Laue-Langevin (ILL), Grenoble, France. For these neutron diffraction measurements, powder samples were filled in a cylindrical vanadium sample container and a standard orange cryostat was used for temperature variation. The measured diffraction patterns were analyzed by using the Rietveld refinement technique (by employing the FULLPROF computer program [40]). The short-range spin-spin correlations were investigated by the reverse Monte Carlo (RMC) method based program SPINVERT [41].

III. RESULTS AND DISCUSSIONS

A. Crystal structure

The crystal structure of $Na_2Co_2TeO_6$ is investigated by combined x-ray and neutron diffraction at room temperature (Fig. 1). The Rietveld analysis reveals that the compound crystallizes in the hexagonal symmetry with space group $P6_322$ (No. 182). The refined values of lattice parameters, atomic positions, and isotropic thermal parameters are given in Table I. The compound $Na_2Co_2TeO_6$ displays a primitive, two-layer hexagonal crystal structure [Fig. 2(a)]. The layers consist of edge-sharing CoO_6 and TeO_6 octahedra within the ab planes. The edge-sharing CoO_6 octahedra form regular
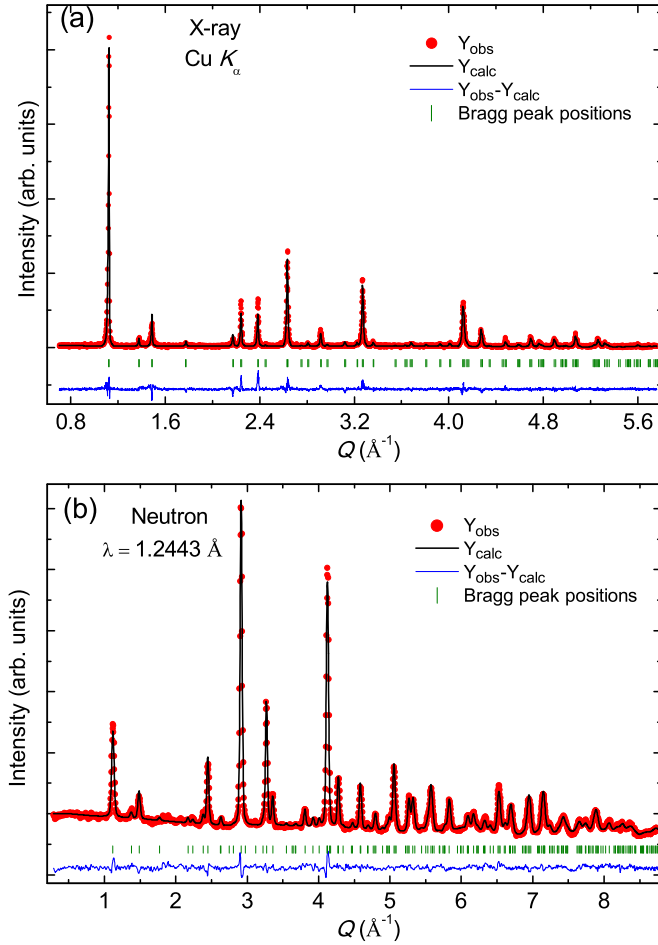
FIG. 1. Experimentally observed (circles) and calculated (solid line through the data points) (a) x-ray and (b) neutron diffraction patterns (intensity vs momentum transfer Q) for $Na_2Co_2TeO_6$ at room temperature. The difference between observed and calculated patterns is shown by the solid lines at the bottom of each panel. The vertical bars indicate the positions of allowed nuclear Bragg peaks.
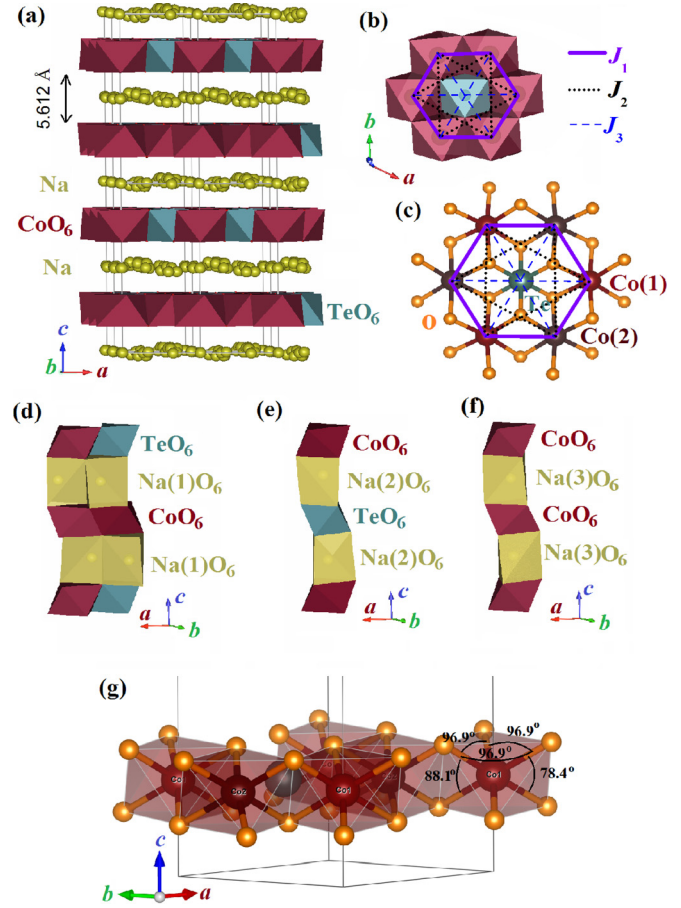

FIG. 2. The crystal structure of $Na_2Co_2TeO_6$. (a) Stacking of the honeycomb layers along the c axis. (b) The honeycomb lattices of Co with NN (J_1), NNN (J_2), and NNNN (J_3) interactions. The TeO_6 octahedra sit at the center of each honeycomb unit. (c) The local crystal structure showing a honeycomb unit with the atomic bonds. (d)–(f) The connection of the magnetic (honeycomb) layers along the c axis by Na(1), Na(2), and Na(3) triangular prisms, respectively. (g) The local crystal structure within the basal plane showing the octahedral environment around the magnetic Co sites. The compression of CoO_6 octahedra along the c axis leads to the decrease of O–Co–O bond angles across the shared edges within the layers.

honeycomb lattices, with TeO_6 octahedra being at the center of the honeycomb lattices [Fig. 2(b)]. Possible exchange paths for the propagation of the higher-order exchange interactions (J_2 and/or J_3) beyond NN (J_1) on this honeycomb lattice are indicated in Figs. 2(b) and 2(c). The details of the possible

superexchange interaction pathways for J_1, J_2, and J_3 are given in Table II. The honeycomb planes are separated along the c axis by an intermediate layer of Na ions. The Na ions are situated within the NaO_6 triangular prisms which connect the honeycomb layers.

In the present crystal structure of $Na_2Co_2TeO_6$, there are two types of symmetry-independent Co sites, one type of Te site, one type of O site, and three independent Na sites. All the Co, Te, and O sites are fully occupied. However, the three Na sites are only partially occupied. They contain different percentages of Na ions [Na(1): ~67%; Na(2): ~25%; Na(3): ~8%]. This leads to a highly disordered distribution of Na ions within the intermediate layers between the honeycomb layers. Moreover, the three Na triangular prismatic sites connect two adjacent honeycomb layers in different ways [Figs. 2(d)–2(f)]. Na(1) triangular prisms share edges with

TABLE I. The Rietveld refined lattice constants, fractional atomic coordinates, and isotropic thermal parameters (B_{iso}) for $Na_2Co_2TeO_6$ at room temperature. Lattice constants $a = 5.2770(2)$ Å, $c = 11.2231(1)$ Å. "*Occ.*" stands for site occupancy.

Atom	Site	x/a	y/b	z/c	B_{iso}	$Occ.$
Co(1)	2b	0	0	0.25	0.32(6)	1.0
Co(2)	2d	2/3	1/3	0.25	0.68(10)	1.0
Te	2c	1/3	2/3	0.25	0.68(10)	1.0
O	12i	0.6446(5)	−0.0260(4)	0.3438(2)	0.98(2)	1.0
Na(1)	12i	0.698(3)	0.056(2)	0.003(2)	1.13(6)	0.225(2)
Na(2)	12i	0.361(9)	0.620(8)	−0.024(2)	1.13(6)	0.085(3)
Na(3)	2a	0	0	0	1.13(6)	0.153(3)

TABLE II. Possible pathways for NN, NNN, and NNNN exchange interactions J_1, and J_2, and J_3, respectively. The Co..Co direct distances, metal oxide (M–O) bond lengths, and bond angles for the exchange interactions J_1, J_2, and J_3 in $Na_2Co_2TeO_6$ at room temperature.

Exchange interaction	Pathways	Co–Co direct distance (Å)	Bond lengths (Å)	Bond angles (deg)
J_1	Co(1)–O–Co(2)	Co(1)–Co(2)=3.044(5)	Co(1)–O=2.094(1) Co(2)–O=2.119(1)	Co(1)–O–Co(2)=92.5(1)
J_2	Co(1)–O–Co(2)–O–Co(1)/ Co(1)–O–Te–O–Co(1)/ Co(1)–O–O–Co(1)	Co(1)–Co(1)=5.272(1)	Co(1)–O=2.094(1) Co(2)–O=2.119(1) Te–O=1.941(1) OO=2.683(2)	Co(1)–O–Co(2)=92.5(1) O–Co(2)–O=174.5(2)/97.4(2)/78.5(1) Co(1)–O–Te=97.9(1) O–Te–O=179.0(1)
	Co(2)–O–Co(1)–O–Co(2)/ Co(2)–O–Te–O–Co(2)/ Co(2)–O–O–Co(2)	Co(2)–Co(2)=5.272(1)	Co(2)–O=2.119(1) Co(1)–O=2.094(1) Te–O=1.941(1) O–O=2.683(2)	Co(2)–O–Co(1)=92.5(1) O–Co(1)–O=173.5(1)/96.9(1)/78.4(1) Co(2)–O–Te=97.0(1) O–Te–O=179.0(1)
J_3	Co(1)–O–Te–O–Co(2)	Co(1)–Co(2)=6.088(5)	Co(1)–O=2.094(1) Co(2)–O=2.119(1) Te–O=1.941(1)	Co(1)–O–Te=97.9(1) Co(2)–O–Te=97.0(1) O–Te–O=179.0(1)

the CoO$_6$ and TeO$_6$ octahedra in the layers above and below, whereas Na(2) triangular prisms share faces with one Co and one Te octahedron in the layers above and below, respectively. On the other hand, Na(3) triangular prisms share faces with two Co octahedra which are situated in the layers above and below, respectively. Therefore, three interlayer couplings with different strengths are possible via the three Na sites. These special structural connections via the intermediate Na layers along with disordered distributions of Na ions play a vital role in the formation of magnetic correlations between the magnetic honeycomb layers along the c axis, as found in our low-temperature neutron diffraction study (discussed later in the magnetic ground-state and short-range magnetic correlations sections).

For both magnetic Co(1) and Co(2) sites, the CoO$_6$ octahedra are formed by six equal bond lengths [2.094(1) Å for Co(1)–O, and 2.119(1) Å for Co(2)–O; (Table III)]. However, the octahedra are found to be flattened along the c axis (perpendicular to the honeycomb layers) [Fig. 2(g)]. Here, all the six O–Co–O bond angles parallel to the basal plane [96.9(1)° for O–Co(1)–O, and 97.4(2)° for O–Co(2)–O; (Table III)] are larger than 90°, whereas the bond angles across the shared edges (perpendicular to the basal plane) [78.4(1)° and 88.1(1)° for O–Co(1)–O, and 78.5(1)° and 86.82(1)° for

O–Co(2)–O; (Table III)] are lower than 90°. For a regular octahedron, all the angles have a value of 90°. This octahedral distortion indicates the presence of a trigonal crystal field at the Co sites.

B. Bulk physical properties

Figure 3(a) shows the temperature-dependent ac susceptibility $\chi(T)$ and heat capacity $C_p(T)$ curves. Both the $\chi(T)$ and $C_p(T)$ curves show anomalies at ~24.8 K indicating the onset of the long-range magnetic ordering. The nature of the anomalies. i.e., a sharp peak in the $\chi(T)$ curve, and a λ-like peak in the $C_p(T)$ curve, suggests an antiferromagnetic-type magnetic ordering. The inset of Fig. 3(a) shows the χT vs T curve. At high temperatures above ~150 K, the temperature-independent constant value of χT indicates a paramagnetic state. With decreasing temperature below ~150 K, the χT curve first deviates from the paramagnetic behavior, and then shows a sharp decrease below ~50 K (well above the T_N ~ 24.8 K), where an onset of short-range magnetic correlations is found in the neutron diffraction study (discussed later).

The temperature-dependent dc susceptibility curves, measured under ZFC and FC conditions, are shown in Figs. 3(b) and 3(c). The ZFC and FC curves show a bifurcation below ~27 K. Two additional anomalies at ~16 and 4 K are also evident. All the features in the ZFC and FC curves are in good agreement with that reported recently by Lefrancois *et al.* [32]. The high-temperature data above 150 K follow a Curie-Weiss behavior. We fit the data (over 150–300 K) with the following equation:

$$\chi = \chi_0 + \frac{C}{(T - \theta_{CW})},$$

where χ_0 is a temperature-independent term that accounts for the diamagnetic and the Van Vleck contributions, C is the Curie constant, and θ_{CW} is the Weiss temperature. The best fit gives $\chi_0 = 0.00106(5)$ emu/mol Co, $\theta_{CW} = -20.9(2)$ K, and $C = 3.85(1)$ emu K/mol Co Oe. The effective moment is estimated

TABLE III. The local crystal structural parameters [bond lengths (Co–O) and bond angles (O–Co–O) within the octahedra] for the two cobalt sites [Co(1) and Co(2)].

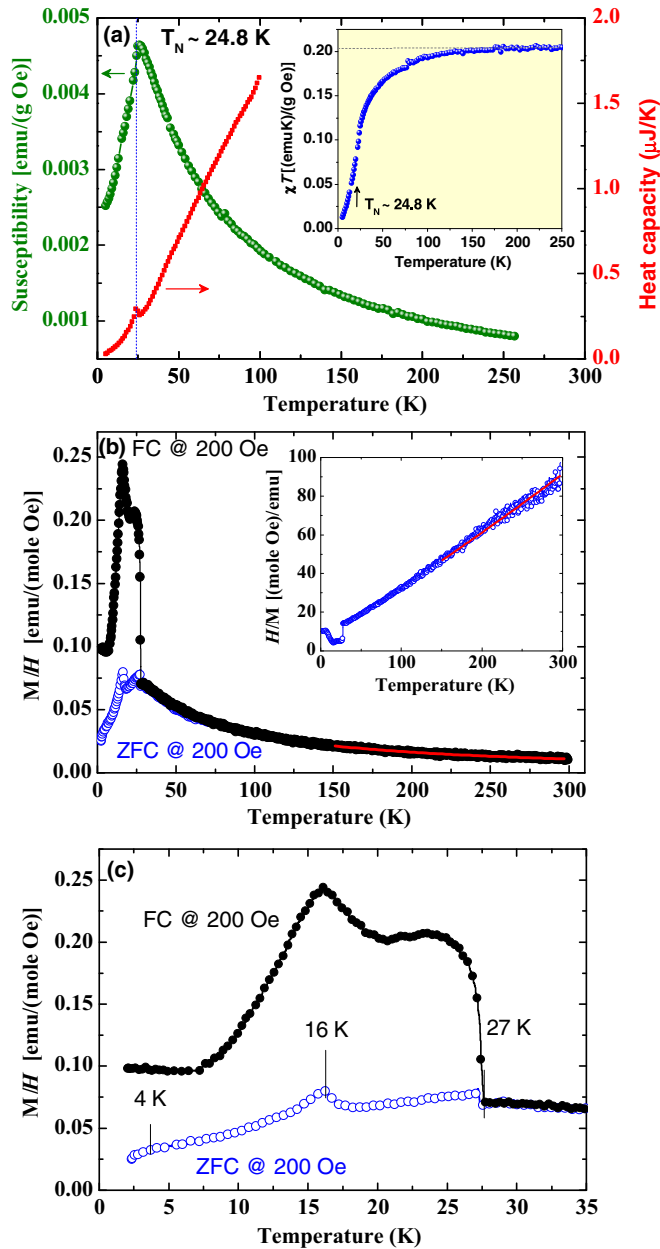|		Co(1)	Co(2)
Bond length (Å)	(Co–O)	2.094(1)	2.119(1)
Bond angle (deg)	(O–Co–O)		
	diagonal	173.5(1)	174.5(2)
	Orthogonal	78.4(1)	78.5(1)
		88.1(1)	86.8(1)
		96.9(1)	97.4(2)

FIG. 3. (a) The temperature-dependent ac susceptibility (χ) and heat capacity (C_p) for $Na_2Co_2TeO_6$. (b) The temperature-dependent dc susceptibility (M/H) curves (ZFC and FC conditions) measured under 200 Oe applied magnetic field. Inset shows the inverse susceptibility curves for the FC conditions. The solid red lines are the Curie-Weiss fit to the data. (c) An enlarged view of the low-temperature ZFC and FC M/H curves.

to be $\mu_{eff} = 5.55\,\mu_B/\mathrm{Co}$. The derived values are also in good agreement with the values reported by Lefrancois *et al.* [32].

Figure 4 shows the isothermal magnetization curves at 2 and 30 K. At 30 K (above $T_N \sim 24.8$ K), the $M(H)$ curve shows a linear-type behavior, whereas at 2 K (in the ordered AFM state; $T < T_N \sim 24.8$ K), the $M(H)$ curve shows an upturn at ~5 T which is further confirmed by its derivative (inset of Fig. 4). A similar M vs H behavior for $Na_2Co_2TeO_6$ was reported earlier by Viciu *et al.* and recently by Lefrancois *et al.* [32,37]. The upturn in the $M(H)$ curve suggests a field induced
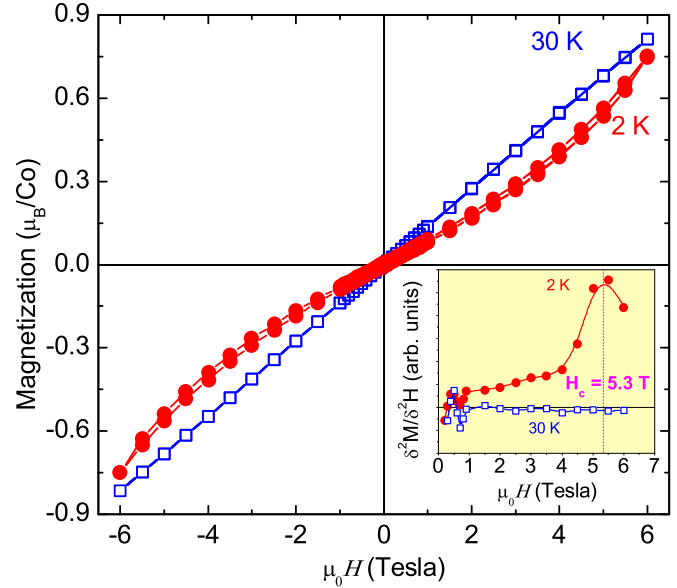

FIG. 4. The isothermal magnetization of $Na_2Co_2TeO_6$ as a function of magnetic field measured at 2 and 30 K. The inset shows the second derivative of magnetization $\delta^2 M/\delta^2 H$ vs H curves.

magnetic transition. Such a field induced transition was reported for several honeycomb antiferromagnets [16,38,42] having zigzag AFM ground states as found for the present compound $Na_2Co_2TeO_6$ (discussed below). In α-RuCl$_3$ [42], the transition was reported to be an order-disorder transition from the zigzag ordered state to a field induced paramagnetic state. A detailed study of the field induced transition in $Na_2Co_2TeO_6$ is beyond the scope of the present work.

C. Magnetic ground state

The nature of the magnetic ground state has been investigated by low-temperature neutron powder diffraction. The neutron diffraction patterns at 30 K (paramagnetic state) and 1.8 K (magnetically ordered state) are shown in Fig. 5. The experimental pattern at 30 K can be refined with the hexagonal crystal structure of $Na_2Co_2TeO_6$ as found at room temperature (Fig. 1). The presence of a few additional weak Bragg peaks from an undetermined secondary phase is also evident. The additional peaks are also evident in the room-temperature pattern (Fig. 1). Nevertheless, these additional peaks do not prevent us from determining the magnetic structure from the analysis of low-temperature neutron diffraction patterns as they remain unchanged with the variation of temperature from 1.8 to 30 K. At 1.8 K, the appearance of a set of additional peaks [marked by stars in Fig. 5(b)] confirms an antiferromagnetic ground state. In order to determine the magnetic structure and the magnetic moments (without any influence from impurity peaks) we use the difference pattern between the patterns measured at 1.8 and 30 K.

All the magnetic peaks at 1.8 K could be indexed with a propagation vector $\mathbf{k} = (1/2\,0\,0)$ with respect to the hexagonal unit cell of the nuclear phase of $Na_2Co_2TeO_6$. To determine the magnetic structure compatible with the space-group symmetry, we carried out representational analysis [43–49] using the program BASIREPS from the FULLPROF package [50,51]. The
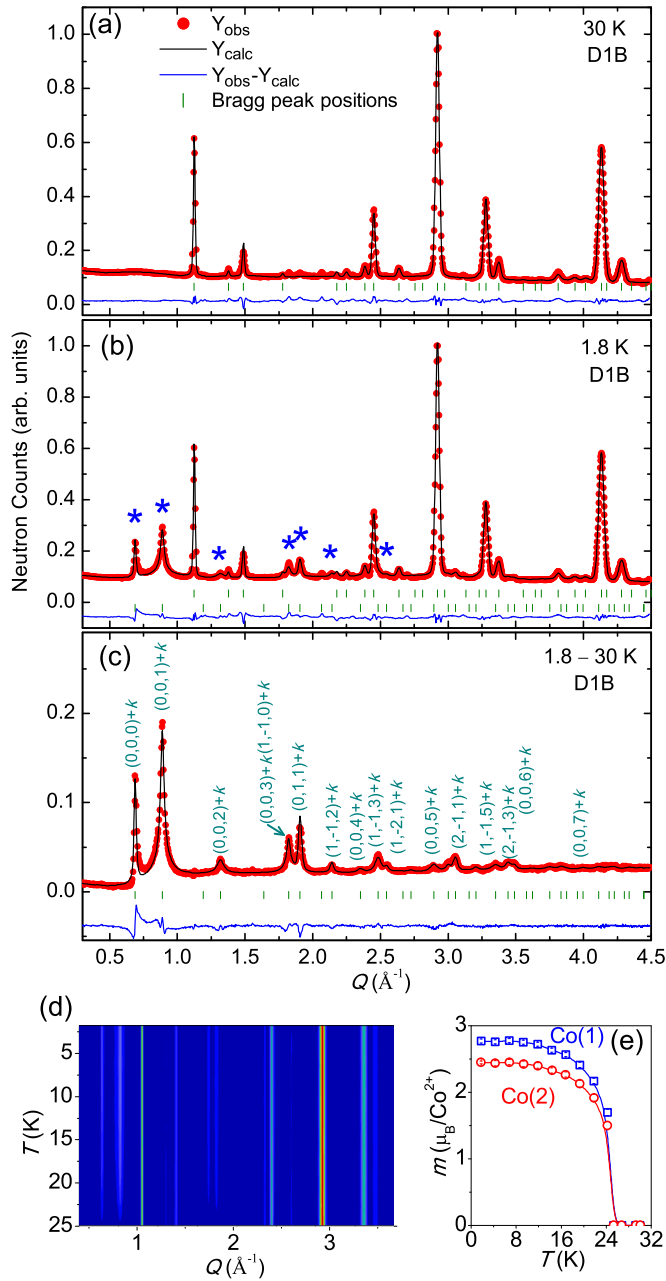
FIG. 5. Experimentally observed (circles) and calculated (solid line through the data points) neutron diffraction patterns ($\lambda = 2.524$ Å) for $Na_2Co_2TeO_6$ at (a) 30 K and (b) 1.8 K. (c) The pure magnetic pattern at 1.8 K after subtraction of nuclear pattern at 30 K. The difference between observed and calculated patterns is shown by the solid line at the bottom of each panel. The vertical bars indicate the positions of allowed nuclear and magnetic Bragg peaks, respectively. (d) The 2D color plot of the temperature-dependent neutron diffraction patterns, showing the appearance of magnetic Bragg peaks below $T_N \sim 24.8$ K. (e) The temperature-dependent ordered magnetic moments for the Co(1) and Co(2) sites. Lines are a guide for the eyes.

symmetry analysis for the propagation vector $\mathbf{k} = (1/200)$ and the space group $P6_322$ gives four nonzero irreducible representations (IRs) (Γs) for both the magnetic sites Co1(2b) and Co2(2d). The magnetic representation Γ_{mag} for both the

TABLE IV. Basis vectors of the magnetic sites Co(1) and Co(2) with the propagation vector $\mathbf{k} = (1/200)$ for $Na_2Co_2TeO_6$. Only the real components of the basis vectors are presented. The four atoms of the nonprimitive basis are defined according to Co(1)–1:(0, 0, 0.25); Co(1)–2: (0, 0, 0.75); and Co(2)–1: (0.6667, 0.3333, 0.2500); Co(2)–2: (–0.6667, –0.3333, 0.7500).

		Basis vectors			
		Site (2b)		Site (2d)	
IRs		Co(1)–1	Co(1)–2	Co(2)–1	Co(2)–2
Γ_1^1	Ψ_1	(210)	(–2–10)	(210)	(–2–10)
Γ_2^1	Ψ_1	(0–10)	(010)	(0–10)	(010)
	Ψ_2	(001)	(001)	(001)	(001)
Γ_3^1	Ψ_1	(0–10)	(0–10)	(0–10)	(0–10)
	Ψ_2	(001)	(00–1)	(001)	(00–1)
Γ_4^1	Ψ_1	(210)	(210)	(210)	(210)

magnetic sites is composed of four IRs as

$$\Gamma_{mag}^{Co(1),Co(2)} = \Gamma_1^1 + \Gamma_2^1 + \Gamma_3^1 + \Gamma_4^1. \qquad (1)$$

The basis vectors of these IRs (the Fourier components of the magnetization) for the two sites Co(1) and Co(2) are given in Table IV. The basis vectors are calculated using the projection operator technique implemented in the BASIREPS program [50].

Out of the above four IRs, the best refinement of the magnetic diffraction pattern is obtained for Γ_2. The refined pure magnetic diffraction pattern as well as the total diffraction pattern at 1.8 K are shown in Figs. 5(c) and 5(b), respectively. For the refinement of the pure magnetic scattering the scale factor and the peak shape parameters were fixed to the values as obtained from the refinement of the purely nuclear data at 30 K. It should also be noted that a *hkl*-dependent peak broadening of the magnetic Bragg peaks, especially for the $(0,0,l) + \mathbf{k}$ peaks, is found. The *hkl*-dependent widths of the magnetic peaks were simulated using the size model 19 of the FULLPROF suite.

The corresponding magnetic structure is shown in Fig. 6. The magnetic moments are pointing along the crystallographic *b* direction. The moments are arranged to form collinear zigzag ferromagnetic chains along the *b* axis within the *ab* plane. Such zigzag FM chains are arranged antiferromagnetically perpendicular to the *b* axis. In this magnetic structure, out of six spins within a honeycomb unit three consecutive spins are arranged along one direction and the other three consecutive spins are arranged opposite to the first three spins. Therefore, for a given spin, out of three nearest neighbors two spins are parallel and one spin is antiparallel. Such antiferromagnetic honeycomb layers are coupled antiferromagnetically along the *c* axis.

The observed zigzag AFM structure of the honeycomb lattice cannot be explained by the sole existence of a J_1 as for this case the ground state should be a Néel-type antiferromagnet having all antiparallel nearest-neighbor spins. The collinear zigzag AFM state in a honeycomb lattice is a result of the order-by-disorder phenomenon as outlined in the Introduction section. As predicted by several theoretical studies, the zigzag
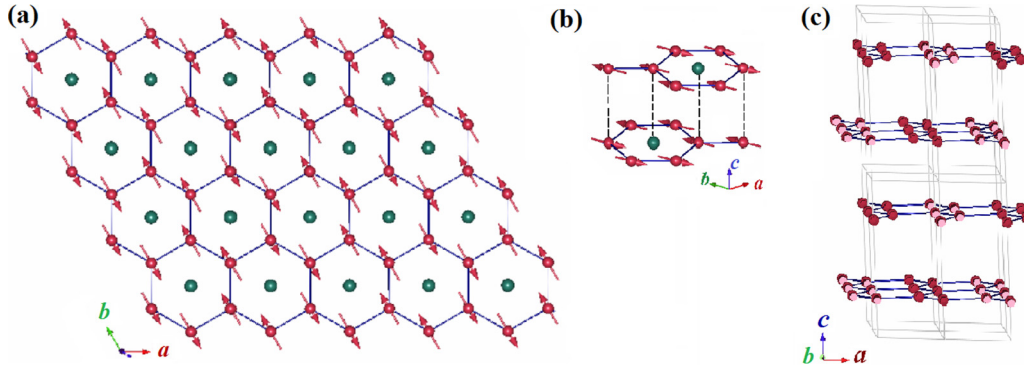
FIG. 6. The magnetic structure of Na$_2$Co$_2$TeO$_6$. (a) The zigzag AFM spin arrangements of Co ions (red spheres) within the honeycomb lattice. Te atoms (green spheres) sit at the center of each honeycomb units. (b) The coupling of the two honeycomb planes along the c axis within a unit cell. (c) The projection of the magnetic structure in the ac plane. The dark and light colored circles represent the moment directions along the $+$ve b axis and $-$ve b axis, respectively. The thin gray lines show the dimension of the unit cells. Te atoms are omitted for clarity.

AFM ground state in a honeycomb lattice is possible in the presence of competing NN, NNN, and NNNN interactions J_1, J_2, and J_3 [1,4]. The recent Monte Carlo study indeed explains the occurrence of zigzag ordering on the basis of the J_1-J_2-J_3 honeycomb model with a weak interlayer coupling in the studied compound Na$_2$Co$_2$TeO$_6$ [32]. Such zigzag AFM ground state has been experimentally reported recently for other frustrated honeycomb compounds Cu$_3$Co$_2$SbO$_6$ [16] and Na$_3$Co$_2$SbO$_6$ [18] with $S = 3/2$, Cu$_3$Ni$_2$SbO$_6$ [16], and Na(Li)$_3$Ni$_2$SbO$_6$ [30] with $S = 1$, and α-RuCl$_3$ [42,52] and Na$_2$IrO$_3$ [53,54] with $j_{\mathrm{eff}} = 1/2$. An experimental study of the spin-wave excitations of the Na$_2$IrO$_3$ compound having the zigzag AFM ground state showed that substantial exchange couplings up to NNNN are required to explain the observed dispersion [54]. On the other hand, for the Na(Li)$_3$Ni$_2$SbO$_6$ [30] and Na$_3$Co$_2$SbO$_6$ [31] compounds with monoclinic crystal structure, the zigzag magnetic ground state was explained on the basis of two types of magnetic exchange interactions J_1 and J_1' with different strengths among the NN magnetic ions within the honeycomb units. The J_1 and J_1' originate from the distorted honeycomb lattice formed by two shorter and four longer bonds, constituted by different bond lengths and bond angles. However, for the present compound Na$_2$Co$_2$TeO$_6$ with hexagonal crystal structure, all the nearest-neighbor bonds are equivalent within the honeycomb units and it is expected that they have equivalent exchange interaction strengths. Therefore, the J_1-J_2-J_3 honeycomb lattice model as discussed above is more suitable for the studied compound Na$_2$Co$_2$TeO$_6$. Moreover, the zigzag AFM ordering in the honeycomb lattice compound Ag$_3$Co$_2$SbO$_6$ was explained recently on the basis of an orbital ordering [33], where two out of six nearest-neighbor exchange interactions are strong, due to direct and superexchange interactions between the half-filled $xz + yz$ orbitals pointing directly to each other. For the other four bonds within the cobalt hexagon, the active half-filled orbitals turn out to be parallel and do not overlap, which results in suppressed (weak) exchange interactions. The presence of an orbital ordering may be possible for the present compound Na$_2$Co$_2$TeO$_6$ where the CoO$_6$ octahedra are found to be flattened along the c axis [Fig. 2 and Table III].

In the present study, the refined ordered moment values were obtained to be $m_{\mathrm{Co(1)}} = 2.77(3)\,\mu_{\mathrm{B}}$/Co^{2+}, and $m_{\mathrm{Co(2)}} =$

2.45(2) μ_{B}/Co^{2+} at 1.8 K. The ordered moment values are found to be significantly reduced from the theoretically expected spin only ordered moment value of 3 μ_{B} for Co^{2+} ions ($3d^7$, $S = 3/2$). It may be noted that in a diffraction measurement only the static components of the magnetic moments are detected, and the reduced moment can be a result of spin fluctuations that originate from spin frustrations. Reduced-order moment values were also reported for other honeycomb compounds having zigzag AFM structures, i.e, 1.9(2) μ_{B}/Ni^{2+} ($S = 1$) for Cu$_3$Ni$_2$SbO$_6$ [16], 2.4(1) μ_{B}/Co^{2+} ($S = 3/2$) for Cu$_3$Co$_2$SbO$_6$ [16], and $0.5 - 0.6(1)\,\mu_{\mathrm{B}}$/Ru^{3+} ($j_{\mathrm{eff}} = 1/2$) for α-RuCl$_3$ [42,52]. The reduction of the ordered moments was attributed to the presence of spin fluctuations as well as of structural stacking faults of the honeycomb layers. In the present compound, the presence of a structural stacking fault is not evident; however, the presence of disorder is clear (discussed below in the next paragraph). The temperature-dependent ordered magnetic moments for both the magnetic sites Co(1) and Co(2) are shown in the inset of Fig. 5(c). Both sublattices order at the same temperature $T_N \sim 24.8$ K, and the ordered moment values increase sharply below T_N and saturate below ~ 10 K.

The temperature dependences of the two low-Q magnetic peaks $(0,0,0) + \mathbf{k}$ and $(0,0,1) + \mathbf{k}$ are shown in Fig. 7. It becomes apparent that the second peak $(0,0,1) + \mathbf{k}$ (originated from both ab plane and c axis out-of-plane magnetic correlations) is broader than the first peak $(0,0,0) + \mathbf{k}$ (arises solely due to the magnetic correlations within the ab plane) for the whole temperature range down to 1.8 K. The estimated widths (FWHM) for these two peaks are plotted as a function of temperature in the inset of Fig. 7. With decreasing temperature, the width of the first peak $(0,0,0) + \mathbf{k}$ decreases sharply just below the T_N, and then becomes constant with a value $\sim 0.018\,\text{\AA}^{-1}$ with further lowering of temperature. The width of the $(0,0,0) + \mathbf{k}$ peak is found to be marginally larger than the instrumental resolution (FWHM = $0.014\,\text{\AA}^{-1}$). On the other hand, the width of the second magnetic peak $(0,0,1) + \mathbf{k}$ is found to be larger ($\sim 0.035\,\text{\AA}^{-1}$ at 24.5 K), and remains constant with decreasing temperature. The whole set of peaks with $(0,0,l) + \mathbf{k}$ indices is also found to be broadened over the full temperature range. At the same time, nuclear Bragg
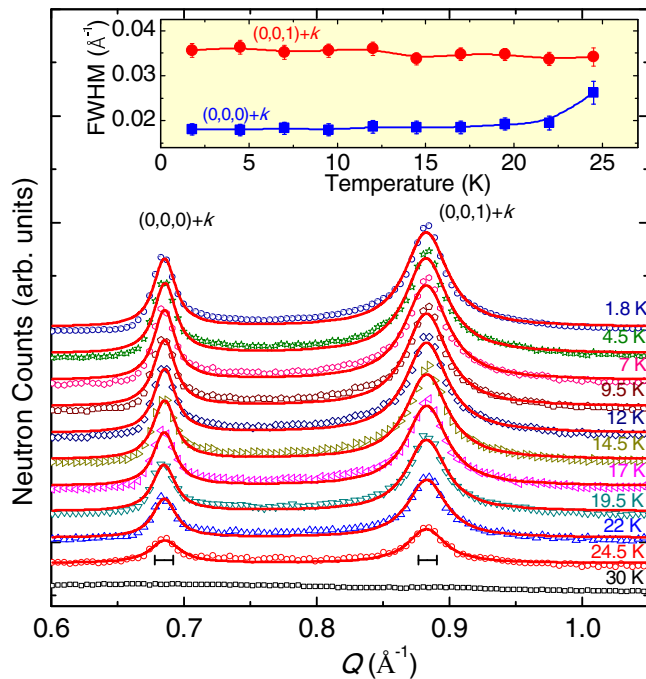
FIG. 7. The temperature evolution of the two low-Q magnetic peaks $(0,0,0) + \mathbf{k}$ and $(0,0,1) + \mathbf{k}$. The solid lines are the fitted curves by a Lorentzian function. The instrumental resolutions are shown by the horizontal bars. Inset: The temperature-dependent peak width (FWHM) of the two magnetic peaks.

peaks are found to be sharp and instrumental resolution limited [Figs. 1, 5, and 8]. In the presence of a structural stacking fault, anomalous broadening of nuclear Bragg peaks and/or appearance of asymmetric wings, leading to a well pronounced inhomogeneous background at different parts of the x-ray and neutron diffraction patterns is expected, as reported for related layered honeycomb compounds $Li_3Ni_2BiO_6$ [25], $Cu_3Ni_2SbO_6$, and $Cu_3Co_2SbO_6$ [16]. Such signatures are absent in the present diffraction patterns at 300 K in the paramagnetic state [Fig. 1]; hence, a structural stacking fault of the honeycomb layers can be ruled out in the present compound. The observed broadening of the set of $(0,0,l) + \mathbf{k}$ magnetic Bragg peaks happens when the magnetic correlation along the c axis is limited. The estimated correlation length along the c axis, by the cylindrical (platelet) shaped crystallites model using the FULLPROF software, is ~ 170 Å.

The limited/restricted magnetic correlations along the c axis may occur in the studied compound $Na_2Co_2TeO_6$ due to the presence of disorder in the intermediate Na layers between the magnetic honeycomb layers. Each disorder disrupts the magnetic coupling between the magnetic ions from the adjacent honeycomb layers, and leads, hence, to a partial breaking of the magnetic correlation along the c axis. The presence of disordered distribution of Na ions among the three sites in the present compound $Na_2Co_2TeO_6$ is evident and already discussed in the crystal structure section. All three Na sites are partially occupied, and these Na triangular prismatic sites connect two adjacent magnetic honeycomb layers differently (by either sharing faces or edges with CoO_6/TeO_6 octahedra) along the c axis [Figs. 2(d)–2(f)]. Therefore, the disordered
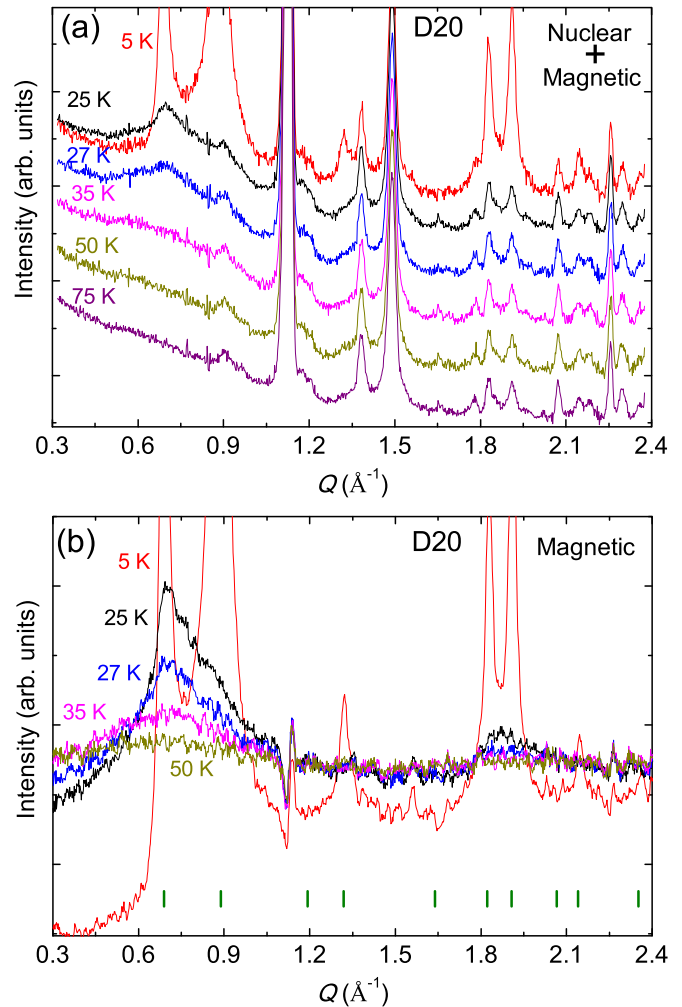

FIG. 8. (a) The experimentally measured neutron diffraction patterns ($\lambda = 2.41$ Å) at 5, 25, 27, 35, 50, and 75 K. (b) The pure magnetic diffraction patterns at 5, 25, 27, 35, and 50 K after subtraction of the 75 K pattern as paramagnetic background. The vertical bars show the magnetic Bragg peak positions in the long-range ordered state below $T_N \sim 24.8$ K. The lower background in the (5–75 K) pattern appears from the subtraction of the Q-dependent paramagnetic scatterings at 75 K arising due to the magnetic form factor of Co^{2+} ions ($S = 3/2$).

statistical distribution of Na ions among the three Na sites strongly affects the magnetic coupling between the honeycomb layers. The present understanding, therefore, implies that the broken magnetic correlations between the honeycomb layers may be present for all structurally related P2-type compounds having partially occupied Na/Li sites. On the other hand, such a phenomenon is expected to be absent in the related O3-type compounds having fully occupied Na/Li sites. However, unavailability of proper data in the literature prevents us from making a direct comparison. Therefore, detailed neutron diffraction experiments on both P2- and O3-type compounds are called for.

D. Short-range magnetic correlations

We now discuss the persistence of short-range magnetic correlations above $T_N \sim 24.8$ K in $Na_2Co_2TeO_6$ which became

visible in the neutron diffraction patterns at 25, 27, 35, and 50 K measured on the high-intensity powder diffractometer D20 at ILL, Grenoble, France, shown in Fig. 8. With decreasing temperature broad diffuse magnetic peaks, corresponding to short-range spin-spin correlations, appear below $\sim$50 K, at a temperature almost twice the Néel temperature T_N. A sharp decrease of the χT values is also found at $T \sim 50$ K (Fig. 3). The broad peaks with maximum at $Q \sim 0.7$ and 1.9 Å^{-1} are situated at the same Q positions where the most intense magnetic Bragg peaks are found below the $T_N \sim 24.8$ K. This indicates that the magnetic periodicity in the short-range state above T_N is similar to the one in the long-range state below T_N. With decreasing temperature, the broad peaks grow monotonically down to T_N, before transforming into magnetic sharp Bragg peaks below T_N.

Similar broad diffuse magnetic peaks in neutron diffraction patterns were reported for several quasi-2D layered spin systems [55–60]. The short-range magnetic correlations were assigned to either 2D or three-dimensional (3D) type depending on the profiles of the diffuse peaks. In case of 2D correlations, the peak shape is an asymmetric sawtooth type which can be defined by a Warren function [55–58]. On the other hand for 3D correlations, the peaks are symmetric, and can be defined by a Lorentzian function [58,59]. In the present case, an asymmetric-type peak shape is evident. However, the peak shape is more complex than the simple Warren function. Moreover, due to the presence of two closely spaced magnetic peaks [i.e., $(0,0,0) + \mathbf{k}$) at $\sim$0.69 Å^{-1}, and $(0,0,1) + \mathbf{k}$ at $\sim$0.89 Å^{-1} for the first diffuse peak] in the present patterns it is difficult to find the dimensionality of the magnetic ordering from the simple fittings of the

analytical functions such as the Warren or/and Lorentzian functions.

To analyze the diffuse scattering data we have used the program SPINVERT [41] which was successfully applied recently to several frustrated magnetic systems showing diffuse magnetic scatterings [61–63]. This program uses a RMC algorithm to fit the experimental powder data (pure magnetic pattern) by a large configuration of spin vectors. A key point of the RMC method is that it is entirely independent of a spin Hamiltonian. Therefore, it is not necessary to assume a form of the Hamiltonian to model the spin correlations. At the same time, it has the limitation that it does not produce a microscopic spin model as an output like the Rietveld method. Compared to other model-independent techniques for the analysis of diffuse neutron scattering (such as simple curve fitting), the RMC approach is superior in both quantity and accuracy of information it provides. Most importantly, this method provides real space spin-spin correlations. Furthermore, the SPINVERT program also calculates scattering profiles in the selected reciprocal planes by using the fitted spin configuration and the crystal structural information. As the program SPINVERT works with orthogonal axes, we have converted the hexagonal unit cell to an equivalent orthorhombic cell having twice the number of magnetic atoms. The transformation matrix for this case is given by

$$\begin{bmatrix} a' \\ b' \\ c' \end{bmatrix} = \begin{bmatrix} 1 & 0 & 0 \\ 1 & 2 & 0 \\ 0 & 0 & 1 \end{bmatrix} \begin{bmatrix} a \\ b \\ c \end{bmatrix}.$$

In the present calculations, a supercell of $10 \times 10 \times 8$ (6400 spins) of the orthorhombic crystal structure is generated,
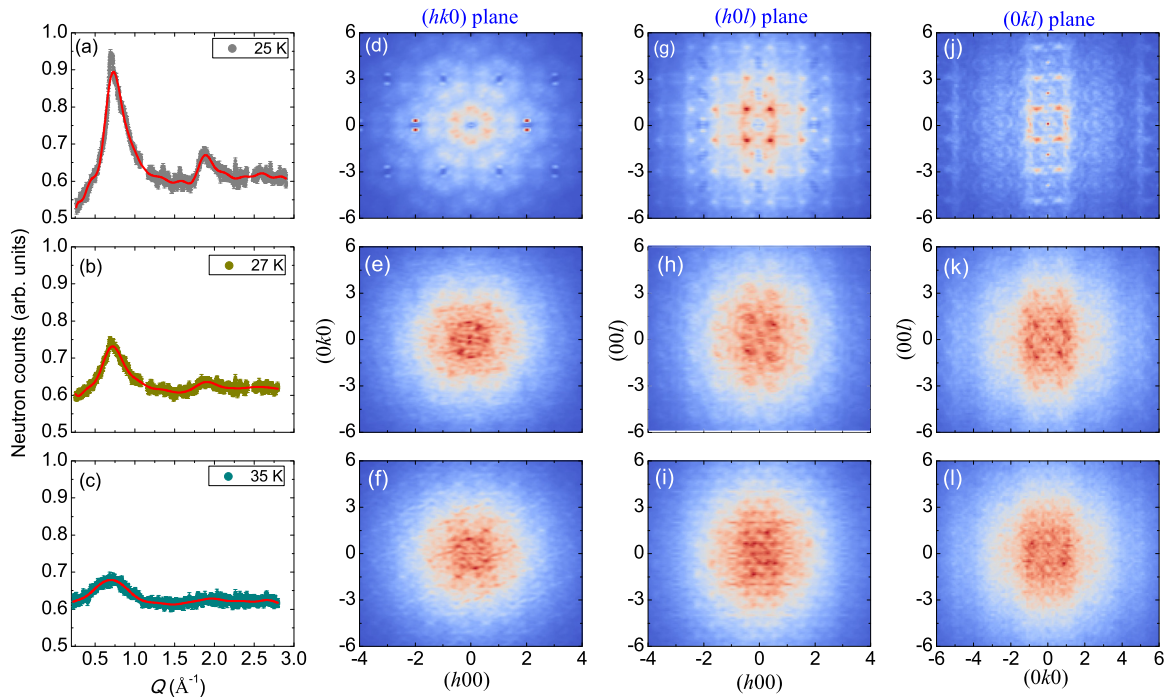

FIG. 9. (a–c) The experimentally measured diffuse magnetic scattering at 25, 27, and 35 K after subtraction of the paramagnetic background at 75 K. The solid lines in each panel are the calculated scattering intensities by the RMC method. (d–l) The reconstructed diffraction patterns in the $(hk0)$, $(h0l)$, and $(0kl)$ scattering planes.

and a randomly oriented magnetic moment is assigned to each magnetic Co site. The positions of spins are fixed at their crystallographic sites throughout the refinement, while their orientations are refined in order to fit the experimental data. A total of 1000 moves per spin is considered for each of the calculations. Ten individual fittings have been performed for each temperature to ensure the robustness of the results.

The calculated diffuse magnetic scattering intensities are shown in Figs. 9(a)–9(c) by the solid lines along with the experimental data (filled circles) at 25, 27, and 35 K. The resulting spin configurations were used to reconstruct the Q dependence of the diffuse scattering in the $(hk0)$, $(h0l)$, and $(0kl)$ scattering planes [Figs. 9(d)–9(l)] by using the SPINDIFF program extension to the SPINVERT program. Rodlike diffuse scattering is evident along the $(00l)$ direction for both the $(h0l)$ and $(0kl)$ scattering planes at all three temperatures. The rodlike feature becomes sharper with decreasing temperature, and gets confined around $h = \pm(2n + 1)/2$ in the $(h0l)$ plane, and $k = \pm(2n + 1)$ in the $(0kl)$ plane, where n is an integer. The positions where the rodlike scattering is found are in agreement with the propagation vector $\mathbf{k} = (1/2 0 0)$ of the magnetic ordered state below T_N. The rodlike scattering reveals that the magnetic correlations are confined within the 2D honeycomb planes (ab plane). In this case no restriction is imposed on the l value, which leads to a rodlike scattering along l. Within the $(hk0)$ plane, the symmetric type of scattering suggests an isotropic correlation within the honeycomb planes. The above results confirm the existence of a 2D magnetic ordering within the honeycomb layers (ab planes) at all temperatures 35, 27, and 25 K above the T_N. The 2D magnetic correlations, confined within the ab plane, are indeed expected from the layered-type crystal structure of the present compound. The crystal structure provides stronger intraplane interactions via the Co–O–Co superexchange interaction pathways, and relatively weak interplane interactions via the Na layers along the c axis. In addition, the disorder in the intermediate Na layers which interrupts the magnetic couplings between honeycomb layers also favors the 2D magnetic correlations within the ab planes.

For further understanding of the nature of the short-range magnetic ordering, the real space spin-pair correlation functions $\langle \vec{S}(0) \cdot \vec{S}(r) \rangle$ are calculated, and shown in Fig. 10. Each data point in Fig. 10 corresponds to a distance between two magnetic sites within the $Na_2Co_2TeO_6$ crystal structure. The spin-pair correlation functions are calculated from the fitted spin configurations by using the program SPINCORREL (an extension of the SPINVERT program). A larger absolute value of $\langle \vec{S}(0) \cdot \vec{S}(r) \rangle$ indicates a stronger preference for a collinear arrangement of the spins, separated by a distance r. The sign of $\langle \vec{S}(0) \cdot \vec{S}(r) \rangle$ indicates whether the spins are parallel $(+)$ or antiparallel $(-)$ to each other. The spin-pair correlations for the present compound (Fig. 10) include both positive and negative values that decrease with the increasing distance (r), and almost vanish at a distance of ~ 12 Å. This is an indication of short-range AFM correlations. The average NN spin-spin correlation $(r = 3.0416$ Å$)$ is found to be FM which is in agreement with the ordered magnetic structure below T_N, where two out of three NN spin-pair correlations
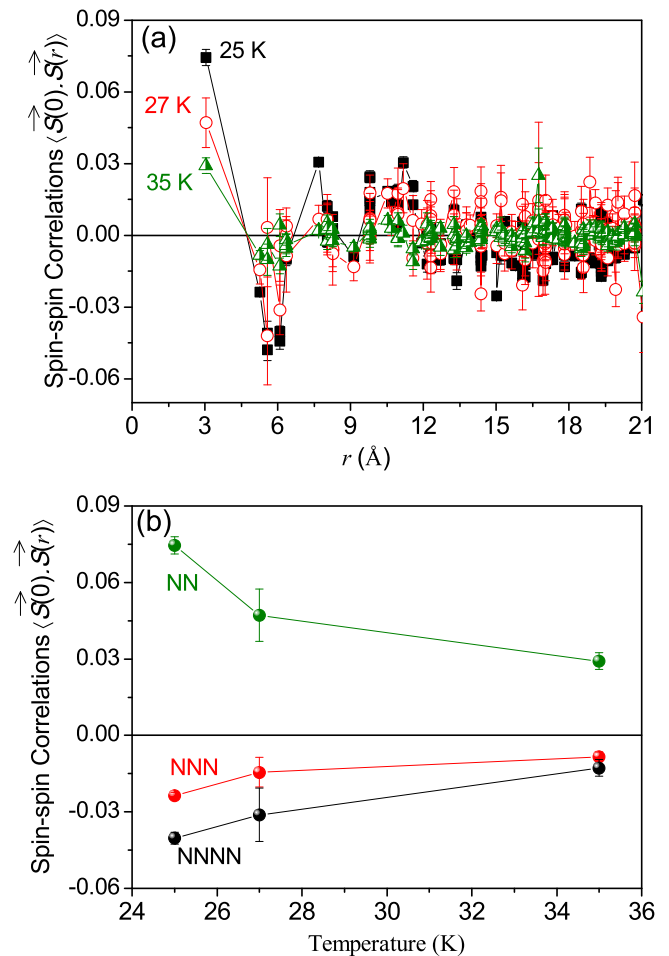

FIG. 10. (a) The radial spin-pair correlation functions at 25, 27, and 35 K corresponding to the fits shown in Figs. 9 (a–c). (b) The temperature-dependent spin-pair correlation functions for the NN, NNN, and NNNN within the honeycomb lattices (in the ab plane).

are FM (Fig. 6). Both the NNN $(r = 5.2679$ Å$)$ and NNNN $(r = 6.0827$ Å$)$ spin-pair correlations within the honeycomb plane are found to be AFM, which is also consistent with the ordered magnetic structure. In this case, four out of six NNN spin-pair correlations are AFM, and all three NNNN spin-pair correlations are AFM (Fig. 6). The temperature dependences of these three correlations are shown in Fig. 10(b). With decreasing temperature, an increase of the correlations without any change in their signs is evident. The spin-pair correlation between the honeycomb planes along the c axis $(r = 5.586$ Å$)$ is found to be AFM, which is again consistent with the ordered magnetic structure below the T_N. All the above results indicate a similar nature of magnetic symmetry in both the short-range (above the T_N) and long-range (below the T_N) ordered states. This indeed reveals that the evolution of magnetic correlations as a function of temperature in $Na_2Co_2TeO_6$ is governed by the intermediate Na layers.

Now we discuss the consequence of having observed a zigzag AFM ground state in the present honeycomb lattice compound $Na_2Co_2TeO_6$. As mentioned earlier such a zigzag magnetic ground state was reported for other honeycomb

lattice compounds α-RuCl$_3$ [42,52] and Na$_2$IrO$_3$ [53] with an effective spin $j_{\text{eff}} = 1/2$. These compounds were reported to situate proximately to the Kitaev spin liquid state [13,64] where the combination of isotropic Heisenberg exchange interaction and anisotropic Kitaev term through strong spin-lattice coupling gives rise to exotic behaviors. Such a situation can be considered for the present compound with magnetic ions Co^{2+} having the similar zigzag AFM ground state. According to the Hund's rules, for the free Co^{2+} $(3d^7)$ ion having seven electrons the total orbital and spin angular momenta are $L = 3$ and $S = 3/2$, respectively. In a distorted (trigonal) octahedral environment (as found for the present compound, and discussed in the Crystal structure section), the orbital and spin degrees of freedoms are entangled by spin-orbit coupling which makes the total angular momentum a conserved quantity. Here, the lowest-lying Kramers doublet of Co^{2+} is well separated from the higher-lying spin-orbit quartet and sextet. Thus the magnetic moment of Co^{2+} can be considered as an effective $j_{\text{eff}} = 1/2$ pseudospin with a large anisotropy [65]. Thus Na$_2$Co$_2$TeO$_6$ could be analogous to the above two compounds; hence there is a possibility to realize the Heisenberg-Kitaev model in this compound as well. The additional advantage of the present compound is that the magnetic coupling between the honeycomb layers could easily be tuned by varying the Na concentrations.

The results of the present work provide an insight into the crystal and magnetic structural correlations in the layered honeycomb lattice compound Na$_2$Co$_2$TeO$_6$. One of the unique aspects of the present work is the understanding of the detailed microscopic magnetic correlations as a function of temperature both above and below the T_N. We have demonstrated that the crystallographically soft Na layers dictate the formation of magnetic correlations. This study provides experimental evidence for the theoretical ideas to explain the nature of the magnetic correlations in a honeycomb lattice, a fertile ground yet to be fully explored. The results of the present study are expected to open up future studies on isostructural compounds having varying spin values and magnetic interaction strengths.

IV. SUMMARY AND CONCLUSIONS

We have investigated the structural and magnetic properties of the frustrated layered honeycomb lattice compound Na$_2$Co$_2$TeO$_6$. Our low-temperature neutron diffraction investigation reveals the existence of a zigzag AFM long-range ordered state below $T_N \sim 24.8$ K which has a restricted correlation along the c axis even deep inside the ordered state at 1.8 K. The restricted correlation along the c axis occurs due to broken magnetic connections, inducted by the disorder distribution of Na ions between three partially occupied sites within the interconnecting layers. Here, Na ions form a NaO$_6$ triangular prism in all these three sites, and connect two adjacent magnetic honeycomb layers differently either by sharing faces or edges with CoO$_6$/TeO$_6$ octahedra along the c axis. Reduced ordered moments of $m_{\text{Co}(1)} = 2.77(3)\,\mu_B/\text{Co}^{2+}$ and $m_{\text{Co}(2)} = 2.45(2)\,\mu_B/\text{Co}^{2+}$ are found at 1.8 K suggesting the persistent spin fluctuations in the ordered state. Our study also shows the presence of short-range magnetic correlations above T_N. The RMC analysis reveals that the dominant spin-pair correlations are within the honeycomb layers (ab plane) with a correlation length about 12 Å at 25 K. The symmetry of the magnetic order is found to be identical in both the short-range and long-range ordered states. This study, thus, provides a comprehensive picture of the microscopic magnetic correlations over the entire temperature range covering the regions both above and below T_N. The present study also demonstrates that the magnetic correlations in Na$_2$Co$_2$TeO$_6$ are dictated by the intermediate nonmagnetic Na layers and provides an in-depth understanding of the crystal and magnetic structural correlations.

[1] J. B. Fouet, P. Sindzingre, and C. Lhuillier, Eur. Phys. J. B **20**, 241 (2001).

[2] J. Oitmaa and R. R. P. Singh, Phys. Rev. B **84**, 094424 (2011).

[3] A. F. Albuquerque, D. Schwandt, B. Hetényi, S. Capponi, M. Mambrini, and A. M. Läuchli, Phys. Rev. B **84**, 024406 (2011).

[4] P. H. Y. Li, R. F. Bishop, D. J. J. Farnell, and C. E. Campbell, Phys. Rev. B **86**, 144404 (2012).

[5] P. H. Y. Li, R. F. Bishop, and C. E. Campbell, Phys. Rev. B **89**, 220408 (2014).

[6] R. F. Bishop, P. H. Y. Li, and C. E. Campbell, Phys. Rev. B **89**, 214413 (2014).

[7] S.-S. Gong, W. Zhu, and D. N. Sheng, Phys. Rev. B **92**, 195110 (2015).

[8] D. C. Cabra, C. A. Lamas, and H. D. Rosales, Phys. Rev. B **83**, 094506 (2011).

[9] H. Zhang, M. Arlego, and C. A. Lamas, Phys. Rev. B **89**, 024403 (2014).

[10] M. Heinrich, H.-A. Krug von Nidda, A. Loidl, N. Rogado, and R. J. Cava, Phys. Rev. Lett. **91**, 137601 (2003).

[11] R. Weht, A. Filippetti, and W. E. Pickett, Europhys. Lett. **48**, 320 (1999).

[12] M. Matsuda, M. Azuma, M. Tokunaga, Y. Shimakawa, and N. Kumada, Phys. Rev. Lett. **105**, 187201 (2010).

[13] J. Chaloupka, G. Jackeli, and G. Khaliullin, Phys. Rev. Lett. **105**, 027204 (2010).

[14] L. Regnault, P. Burlet, and J. Rossat-Mignod, Physica B+C **86–88**, 660 (1977).

[15] L. Regnault, J. Henry, J. Rossat-Mignod, and A. D. Combarieu, J. Magn. Magn. Mater. **15–18**, 1021 (1980).

[16] J. H. Roudebush, N. H. Andersen, R. Ramlau, V. O. Garlea, R. Toft-Petersen, P. Norby, R. Schneider, J. N. Hay, and R. J. Cava, Inorg. Chem. **52**, 6083 (2013).

[17] O. Smirnova, M. Azuma, N. Kumada, Y. Kusano, M. Matsuda, Y. Shimakawa, T. Takei, Y. Yonesaki, and N. Kinomura, J. Am. Chem. Soc. **131**, 8313 (2009).

[18] N. Onishi, K. Oka, M. Azuma, Y. Shimakawa, Y. Motome, T. Taniguchi, M. Hiraishi, M. Miyazaki, T. Masuda, A. Koda, K. M. Kojima, and R. Kadono, Phys. Rev. B **85**, 184412 (2012).

[19] S. Okubo, F. Elmasry, W. Zhang, M. Fujisawa, T. Sakurai, H. Ohta, M. Azuma, O. A. Sumirnova, and N. Kumada, J. Phys.: Conf. Ser. **200**, 022042 (2010).

[20] A. Möller, U. Löw, T. Taetz, M. Kriener, G. André, F. Damay, O. Heyer, M. Braden, and J. A. Mydosh, Phys. Rev. B **78**, 024420 (2008).

[21] S. Derakhshan, H. L. Cuthbert, J. E. Greedan, B. Rahaman, and T. Saha-Dasgupta, Phys. Rev. B **76**, 104403 (2007).

[22] J. Xu, A. Assoud, N. Soheilnia, S. Derakhshan, H. L. Cuthbert, J. E. Greedan, M. H. Whangbo, and H. Kleinke, Inorg. Chem. **44**, 5042 (2005).

[23] Y. Miura, R. Hirai, Y. Kobayashi, and M. Sato, J. Phys. Soc. Jpn. **75**, 084707 (2006).

[24] E. A. Zvereva, M. A. Evstigneeva, V. B. Nalbandyan, O. A. Savelieva, S. A. Ibragimov, O. S. Volkova, L. I. Medvedeva, A. N. Vasiliev, R. Klingeler, and B. Buechner, Dalton Trans. **41**, 572 (2012).

[25] R. Berthelot, W. Schmidt, S. Muir, J. Eilertsen, L. Etienne, A. W. Sleight, and M. A. Subramanian, Inorg. Chem. **51**, 5377 (2012).

[26] M. A. Evstigneeva, V. B. Nalbandyan, A. A. Petrenko, B. S. Medvedev, and A. A. Kataev, Chem. Mater. **23**, 1174 (2011).

[27] J. Roudebush and R. Cava, J. Solid State Chem. **204**, 178 (2013).

[28] M. Schmitt, O. Janson, S. Golbs, M. Schmidt, W. Schnelle, J. Richter, and H. Rosner, Phys. Rev. B **89**, 174403 (2014).

[29] A. K. Bera, S. M. Yusuf, A. Kumar, and C. Ritter, arXiv:1608.07389v1.

[30] E. A. Zvereva, M. I. Stratan, Y. A. Ovchenkov, V. B. Nalbandyan, J.-Y. Lin, E. L. Vavilova, M. F. Iakovleva, M. Abdel-Hafiez, A. V. Silhanek, X.-J. Chen, A. Stroppa, S. Picozzi, H. O. Jeschke, R. Valentí, and A. N. Vasiliev, Phys. Rev. B **92**, 144401 (2015).

[31] C. Wong, M. Avdeev, and C. D. Ling, J. Solid State Chem. **243**, 18 (2016).

[32] E. Lefrancois, M. Songvilay, J. Robert, G. Nataf, E. Jordan, L. Chaix, C. V. Colin, P. Lejay, Hadj-Azzem, R. Ballou, and V. Simonet, Phys. Rev. B **94**, 214416 (2016).

[33] E. A. Zvereva, M. I. Stratan, A. V. Ushakov, V. B. Nalbandyan, I. L. Shukaev, A. V. Silhanek, M. Abdel-Hafiez, S. V. Streltsov, and A. N. Vasiliev, Dalton Trans. **45**, 7373 (2016).

[34] W. Schmidt, R. Berthelot, L. Etienne, A. Wattiaux, and M. A. Subramanian, Mater. Res. Bull. **50**, 292 (2014).

[35] N. Bhardwaj, A. Gupta, and S. Uma, Dalton Trans. **43**, 12050 (2014).

[36] W. Schmidt, R. Berthelot, A. Sleight, and M. Subramanian, J. Solid State Chem. **201**, 178 (2013).

[37] L. Viciu, Q. Huang, E. Morosan, H. Zandbergen, N. Greenbaum, T. McQueen, and R. Cava, J. Solid State Chem. **180**, 1060 (2007).

[38] E. M. Seibel, J. H. Roudebush, H. Wu, Q. Huang, M. N. Ali, H. Ji, and R. J. Cava, Inorg. Chem. **52**, 13605 (2013).

[39] R. Berthelot, W. Schmidt, A. Sleight, and M. Subramanian, J. Solid State Chem. **196**, 225 (2012).

[40] J. Rodriguez-Carvajal, Physica B **192**, 55 (1993).

[41] J. A. M. Paddison, J. R. Stewart, and A. L. Goodwin, J. Phys.: Condens. Matter **25**, 454220 (2013).

[42] R. D. Johnson, S. C. Williams, A. A. Haghighirad, J. Singleton, V. Zapf, P. Manuel, I. I. Mazin, Y. Li, H. O. Jeschke, R. Valentí, and R. Coldea, Phys. Rev. B **92**, 235119 (2015).

[43] E. F. Bertaut, J. Appl. Phys. **33**, 1138 (1962).

[44] E. F. Bertaut, Acta Crystallogr., Sect. A **24**, 217 (1968).

[45] E. F. Bertaut, J. Magn. Magn. Mater. **24**, 267 (1981).

[46] Y. A. Izyumov, V. E. Naish, and R. P. Ozerov, *Neutron Diffraction of Magnetic Materials* (Consultants Bureau, New York, 1991).

[47] C. Bradley and A. Cracknell, *The Mathematical Theory of Symmetry in Solids* (Clarendon Press, Oxford, 1972).

[48] A. Cracknell, *Magnetism in Crystalline Materials* (Pergamon Press, Oxford, 1975).

[49] A. S. Wills, Phys. Rev. B **63**, 064430 (2001).

[50] J. Rodriguez-Carvajal, BASIREPS: a program for calculating irreducible representations of space groups and basis functions for axial and polar vector properties. Part of the FULLPROF suite of programs, www.ill.eu/sites/fullprof/.

[51] C. Ritter, Solid State Phenom. **170**, 263 (2011).

[52] C. Ritter, J. Phys.: Conf. Ser. **746**, 012060 (2016).

[53] F. Ye, S. Chi, H. Cao, B. C. Chakoumakos, J. A. Fernandez-Baca, R. Custelcean, T. F. Qi, O. B. Korneta, and G. Cao, Phys. Rev. B **85**, 180403 (2012).

[54] S. K. Choi, R. Coldea, A. N. Kolmogorov, T. Lancaster, I. I. Mazin, S. J. Blundell, P. G. Radaelli, Y. Singh, P. Gegenwart, K. R. Choi, S.-W. Cheong, P. J. Baker, C. Stock, and J. Taylor, Phys. Rev. Lett. **108**, 127204 (2012).

[55] J. W. Lynn, T. W. Clinton, W.-H. Li, R. W. Erwin, J. Z. Liu, K. Vandervoort, and R. N. Shelton, Phys. Rev. Lett. **63**, 2606 (1989).

[56] H. Zhang, J. W. Lynn, and D. E. Morris, Phys. Rev. B **45**, 10022 (1992).

[57] S. M. Yusuf, A. K. Bera, N. S. Kini, I. Mirebeau, and S. Petit, Phys. Rev. B **82**, 094412 (2010).

[58] S. M. Yusuf, J. M. De Teresa, P. A. Algarabel, M. D. Mukadam, I. Mirebeau, J.-M. Mignot, C. Marquina, and M. R. Ibarra, Phys. Rev. B **74**, 184409 (2006).

[59] A. K. Bera, S. M. Yusuf, and I. Mirebeau, J. Phys.: Condens. Matter **23**, 426005 (2011).

[60] A. K. Bera, S. M. Yusuf, and S. Banerjee, Solid State Sci. **16**, 57 (2013).

[61] J. A. M. Paddison and A. L. Goodwin, Phys. Rev. Lett. **108**, 017204 (2012).

[62] G. J. Nilsen, C. M. Thompson, G. Ehlers, C. A. Marjerrison, and J. E. Greedan, Phys. Rev. B **91**, 054415 (2015).

[63] J. A. M. Paddison, S. Agrestini, M. R. Lees, C. L. Fleck, P. P. Deen, A. L. Goodwin, J. R. Stewart, and O. A. Petrenko, Phys. Rev. B **90**, 014411 (2014).

[64] A. Banerjee, C. A. Bridges, J.-Q. Yan, A. A. Aczel, L. Li, M. B. Stone, G. E. Granroth, M. D. Lumsden, Y. Yiu, J. Knolle, S. Bhattacharjee, D. L. Kovrizhin, R. Moessner, D. A. Tennant, D. G. Mandrus, and S. E. Nagler, Nat. Mater. **15**, 733 (2016).

[65] A. Abragam and B. Bleaney, *Electron Paramagnetic Resonance of Transition Ions* (Clarendon Press, Oxford, UK, 1970).